

Robust High-Performance Disturbance Rejection for an Uncertain Inverted Double Pendulum

Uwe Mackenroth

Abstract— This paper deals with some new aspects of the well-known double pendulum experiment (sometimes also denoted as pendubot). It becomes challenging if it is made uncertain by adding suitable mechanic and electronic devices and if additionally the performance requirements are taken to the limit. It will be proposed how this can be achieved. The performance for the upward directed double pendulum is measured in terms of disturbance rejection properties. Several controllers are designed: pole placement, LQ, \mathcal{H}_2 , \mathcal{H}_∞ and μ . They are compared with respect to their performance and robustness properties. The main performance limitation comes from additional high-frequency dynamics of the plant which are found by identification. Additionally, the dynamics of the actuator are made uncertain by adding a suitable electronic circuit at the input of the pwm amplifier. To handle this challenging situation, a μ controller will be designed which has remarkable robustness and performance properties. In a further part of the experiment, a weight with a spring is mounted at the double pendulum. This leads to an oscillatory disturbance and moreover to a change of the dynamics of the plant so that excellent robustness properties of the controller are required.

I. INTRODUCTION

IN the last two decades, a tremendous progress concerning controller design and analysis methods was made. For the students or practitioners working in industries the question arises which of these modern methods should be chosen and how they should be applied. A convincing way to get familiar with the specific advantages and disadvantages of a method is to apply it to a suitable laboratory experiment. Even for a researcher such an experiment is of great value because it puts him into a position to compare his method with already existing ones. For this reason, there is a need for benchmark laboratory experiments which on the one hand are easily accessible and on the other hand are difficult enough to characterize the specific properties of the applied design method.

The laboratory experiment under consideration deals with stabilization and disturbance rejection for an inverted double pendulum. This problem is not new and there are various papers dealing with it, compare for example [2], [3], and [4]. The difference from these papers is that we add a mechanical and an electrical uncertainty to the plant and

Manuscript received August 22, 2007. U. Mackenroth is with the Fachhochschule Lübeck (University of Applied Sciences), Fachbereich Maschinenbau und Wirtschaftsingenieurwesen, 23562 Lübeck, Germany, e-mail: mackenroth@fh-luebeck.de.

that we try to achieve maximum performance by the controller. The performance will be measured in terms of rejecting a strong disturbance as good as possible. These hard requirements can not be fulfilled by "simple" controllers designed by pole placement or linear quadratic optimization. It is necessary to synthesize sophisticated \mathcal{H}_∞ or μ controllers to get a satisfactory result. A paper dealing with a similar intention for a simple pendulum is [5].

In Sect. 2, we first describe the dynamics of the plant by using the Euler-Lagrange method. The dynamical quantities are the two deflection angles of the pendulum and the spring deflection. It will be found experimentally that there are additional high-frequency dynamics. Later, we will see that these dynamics play a key role for controller design when hard performance requirements are imposed.

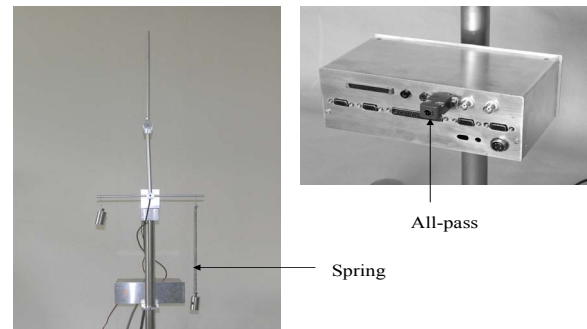


Fig. 1.1: Pendulum with spring and electronic unit with uncertainty

In Sect. 3, a pole placement, a LQ and a \mathcal{H}_2 controller will be designed. All three controllers are capable to stabilize the pendulum but their ability to reject a constant disturbance at the plant input differs considerably. Performance limitations are the limited current and the additional high-frequency dynamics. The best controller is the \mathcal{H}_2 controller. In Sect. 4, a \mathcal{H}_∞ controller design will be tried to obtain further improvements. By introducing a weight for the transfer function for the disturbance, considerably better disturbance rejection properties in comparison to the \mathcal{H}_2 controller can be achieved. Then we add further uncertainty by implementing an all-pass before the pwm amplifier. This degrades the performance of the \mathcal{H}_∞ controller. Specifying an uncertainty model and using the D-K iteration, it is possible to design a μ controller which has approximately the same performance for the nominal plant as the \mathcal{H}_∞ controller but whose performance is only mildly degraded by the electronic circuit.

In the last part of the experiment, the constant disturbance is replaced by an oscillatory one which is realized by a moving mass which is mounted at a spring (Sect. 5). Strictly speaking, the additional spring-mass system is not a disturbance but a further uncertainty of the plant. Controller design is done for the system without the spring and the spring is taken into account by choosing suitable weights. A comparable industrial situation arises for the Hubble space telescope: Here, the solar arrays cause structural vibrations of the telescope and have to be suppressed by the controller (cf. [6]).

II. MATHEMATICAL MODEL OF THE PLANT

Nonlinear pendulum dynamics. The dynamical quantities are the deflection angles φ and ψ and the deflection z of the spring, cf. Fig. 2.1. In a complete rigorous approach, a fourth variable would be needed, namely the angle α which describes the lateral oscillations of the additional pendulum which is formed by the spring, the rod and the mass m_0 . These oscillations are visible in the experiment but the effect on the double pendulum is very small if a motion of the double pendulum near a position where the rod is nearly horizontal is considered. Then the moment caused by the side motion depends on $\cos \alpha$ which is 1 in a first order approximation. If the dynamics are linearized, the side motion is completely decoupled from the rest of the pendulum and needs not to be considered for control purposes. For this reason, we assume $\alpha = 0$.

Let (cf. Fig. 2.1)

$$\begin{aligned} J_1 &= J_{1S} + m_1 l_1^2 + m_2 L^2 + 2m_0 L_0^2 \\ J_2 &= J_{2S} + m_2 l_2^2. \end{aligned}$$

Define a generalized mass matrix by (with $\delta = \psi - \varphi$)

$$M(q) = \begin{pmatrix} J_2 & m_2 l_2 L \cos \delta & 0 \\ m_2 l_2 L \cos \delta & J_1 & -m_0 L_0 \cos \varphi \\ 0 & -m_0 L_0 \cos \varphi & m_0 \end{pmatrix}.$$

Then the kinetic energy and the potential energy are (with $q = (\psi \ \varphi \ z)^T$ as the vector of the generalized coordinates)

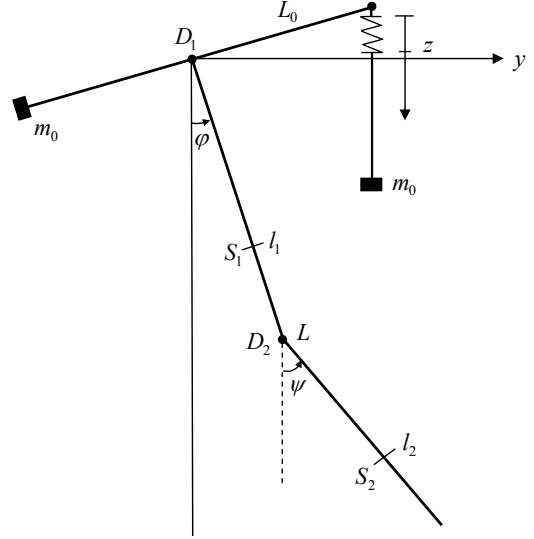
$$K(q, \dot{q}) = \frac{1}{2} \dot{q}^T M(q) \dot{q}$$

$$P(q) = -(m_1 l_1 + m_2 L) g \cos \varphi - m_2 l_2 g \cos \psi + \frac{1}{2} c z^2.$$

The friction torque about D_1 is $M_{f\varphi}$, and the friction torque about D_2 is $M_{f\psi}$. Both are the sum of viscous and Coulomb friction:

$$\begin{aligned} M_{f\varphi} &= r_{\varphi c} \text{sign}(\varphi) + r_{\varphi v} \dot{\varphi} \\ M_{f\psi} &= r_{\psi c} \text{sign}(\psi - \varphi) + r_{\psi v} (\psi - \dot{\varphi}). \end{aligned}$$

The motor induces a torque M_a about D_1 . It can be written as $M_a = c_a i_a = c_a k_i u = k u$ where u is the input



- S_1, S_2 : Centers of gravity of the T-shaped pendulum 1 and of pendulum 2, resp.
- L : Distance of D_1 and D_2 ,
- l_1, l_2 : Distances of D_1 and S_1 and of D_2 and S_2 , resp.
- m_1, m_2 : Masses of pendulum 1 and of pendulum 2, resp.
- J_{1S}, J_{2S} : Moments of inertia of the T-shaped pendulum 1 about S_1 and of pendulum 2 about S_2 , resp.
- $2L_0$: Length of the horizontal bar
- c : Spring constant

Fig. 2.1: Dynamical quantities and constants for the double pendulum

voltage of the pwm amplifier and where c_a, k_i are constants (and $k = c_a k_i$). We denote the vector with the components $0, 0, M_a$ also by M_a . Let M_f be the vector with the components $M_{f\psi}, M_{f\varphi}, 0$. Define a matrix $C(q, \dot{q})$ and a vector $g(q)$ by

$$C(q, \dot{q}) = \begin{pmatrix} 0 & m_2 l_2 L \dot{\varphi} \sin \delta & 0 \\ -m_2 l_2 L \dot{\psi} \sin \delta & 0 & 0 \\ 0 & m_0 L_0 \dot{\varphi} \sin \varphi & 0 \end{pmatrix}$$

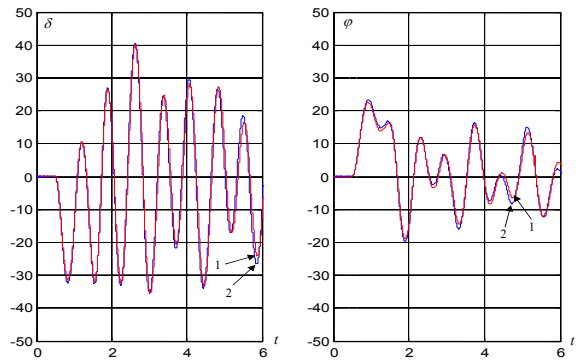


Fig. 2.2: Step response for the double pendulum (curve 1: measured signal, curve 2: simulated signal)

$$g(q) = \begin{pmatrix} m_2 l_2 g \sin \psi \\ (m_1 l_1 + m_2 L) g \sin \varphi \\ cz \end{pmatrix}.$$

Then the Euler-Lagrange equation can be written in the form

$$M(q)\ddot{q} + C(q, \dot{q})\dot{q} + g(q) + M_r(\dot{q}) = M_a. \quad (2.1)$$

With this equation it is possible to build up a SIMULINK model. In the experiments, it runs in real-time in parallel to the hardware. Figure 2.2 shows the measured and simulated quantities for a step response. It can be seen from the figure that the simulation model is very accurate.

Linear model of the plant. If no external torque is exerted on the pendulum, it has four equilibrium points (ψ_0, φ_0) . We are interested in the equilibrium point where both links are directed upwards (the up-up position). It is a routine task to linearize (2.1) and to compute the transfer functions. For the up-up position and the double pendulum without spring, the transfer functions from u to δ and u to φ are (if friction is neglected)

$$G_\delta(s) = k_1 \frac{(s - \omega_{z1})(s + \omega_{z1})}{(s - \omega_1)(s + \omega_1)(s - \omega_2)(s + \omega_2)},$$

$$G_\varphi(s) = k_2 \frac{(s - \omega_{z2})(s + \omega_{z2})}{(s - \omega_1)(s + \omega_1)(s - \omega_2)(s + \omega_2)}$$

(with ω_{z1} close to ω_1 and ω_{z2} close to ω_1). Thus the plant has two real poles in the right half-plane and non-minimum phase behavior. The transfer function from u to $(\delta, \varphi)^T$ will be denoted by G_{id} .

Identified high-frequency dynamics of the plant. The simplest stabilizing controller for the double pendulum uses state feedback and can be designed by pole placement, for example. If (2.1) would exactly describe the full dynamic

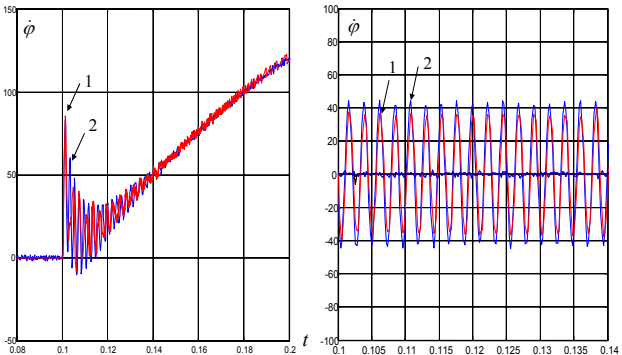


Fig. 2.3: Step response (left-hand figure) and response to a sinusoidal input with $\omega = 2470 \text{ s}^{-1}$ (right-hand figure). Curve 1: measured signal, curve 2: simulated signal

of the plant, the only performance limitation would be caused by actuator saturation. Surprisingly, the real plant becomes unstable before the actuator runs into saturation and this behavior is not reflected in the mathematical model up to now. In the next section, we take a closer look at this instability. In any case, from this observation it can be concluded that there must exist unmodeled high-frequency dynamics in the plant. One possible source might be the pwm amplifier. The pwm amplifier shows a behavior which is close to that of a PT_1 system with a very small time constant, namely $T_{pwm} = 0.00035 \text{ s}$, but this time lag is not the explanation of the instability.

The goal is to find a mathematical model of this unknown part of the dynamics. The most convincing proof for the existence of unmodeled dynamics is found in this case by applying sinusoidal oscillations to the real plant and to compare the measured output with the simulated output. By this way, it can be seen that the real plant has a resonance peak at 2600 rad/s. At this frequency, the measured amplitude is approximately 50dB larger than that predicted by the model. A second approach is to look at the step responses for a short time interval with a small sampling period. The measured step response shows for some milliseconds an oscillatory behavior. The next step is to complete the ideal transfer function G_{id} by a transfer function such that the series combination approximately has the same behavior as the real plant. A good choice is

$$H(s) = \frac{(1 + k_I)s^2 + 2d_I\omega_I s + \omega_I^2}{s^2 + 2d_I\omega_I s + \omega_I^2}. \quad (2.3)$$

The numerical values are $\omega_I = 2600 \text{ s}^{-1}$, $k_I = 190$, and $d_I = 0.04$. We denote these dynamics as identified high-frequency dynamics (IdHFDyn). Thus the IdHFDyn contribute a transfer functions with a pair of zeros and a pair of poles near to the imaginary axis. Figure 2.3 shows the simulated and measured responses of the plant to a step and a sinusoidal input. It should be noted that without the IdHFDyn, the response to a harmonic oscillation in Fig. 2.3 would be close to zero.

III. DESIGN OF A POLE PLACEMENT, A LQ AND A \mathcal{H}_2 CONTROLLER

The main goal of the experiment is to design various controllers and to compare their quality with respect to performance and robustness. Since the main concern for the pendulum is stabilization, it is natural to measure performance by the ability of the controller to reject a disturbance. We start with a large constant disturbance and require that the disturbance has to be rejected as quickly as possible.

Controller design by pole placement. The simplest controller is designed by pole placement and feeds back the measured angles δ, φ and the rates $\dot{\delta}, \dot{\varphi}$. Since the rates

are not directly measured, they are obtained by using a differentiator. Because we want to reject a constant disturbance without a stationary control error, an integrator is needed. The controller then can be written as

$$\hat{u} = k_1 \frac{1 + T_{D1}s}{1 + T_{01}s} \hat{\delta} + k_2 \frac{1 + T_{D2}s}{1 + T_{02}s} \hat{\varphi} + \frac{k_3}{s} (\hat{\varphi}_0 - \hat{\varphi}).$$

A natural choice for the closed-loop poles is to leave the stable poles as they are and to mirror the unstable poles at the imaginary axis. If a larger bandwidth is required, a possible choice for the closed-loop poles is

$$s_{1,2} = -\lambda\omega_1, s_{3,4} = -\lambda\omega_2, s_5 = -\omega_I$$

with a factor λ and a number $\omega_I > 0$. The pole s_5 corresponds to the integrator. For $\lambda \geq 1$, the Nyquist curve for such a controller with $T_{01} = T_{02} = 0$ has a perfect behavior: It avoids a circle with center -1 and radius 1 . Thus, if robustness is measured by the Nyquist criterion, the closed-loop system is very robust (cf. [3], Chap. 6.3). For $\lambda < 1$, the Nyquist curve comes closer to the point -1 . The bandwidth of the closed-loop system increases if λ increases. On the other hand, the control effort increases very quickly if λ increases.

The two differentiators may be interpreted as reduced observers for the rates. The design parameters are the time constants T_{01} and T_{02} . If they are very small, the control has a sharp peak at the beginning of the control action. If they increase, the closed-loop system gets at least one complex conjugate pole pair with a possibly small damping. We choose $T_{01} = \gamma T_{D1}$ and $T_{02} = \gamma T_{D2}$ with a suitable number $\gamma < 1$ and ω_I equal to the minimum of ω_1 and ω_2 . The design parameters are now λ and γ . A reasonable choice is $\lambda = 1$ and $\gamma = 0.05$.

Surprisingly, with these choices the real closed-loop system is unstable whereas the controller in the simulation works very well. This was the reason for seeking for additional high frequency dynamics. If the pendulum dynamics is completed by a suitable transfer function of the form (2.3), the closed-loop system becomes unstable in the simulation, too. An acceptable controller is obtained for the choice $\lambda = 0.5$ and $\gamma = 0.05$.

An interesting situation occurs if the system is driven at the stability limit. Then it may occur that the linearized closed-loop system is unstable whereas the nonlinear system is stable in the sense of Lyapunov, for the hardware as well as for the simulation! The control oscillates between the maximum possible values but the pendulum remains in the upward position. Figure 3.1 shows the measured and simulated quantities for such a case.

LQ controller design. Here, the output for controller design is $(Cx \sqrt{r}u)^T$. We choose

$$C = (L \ 0 \ l_2 \ 0 \ q_e).$$

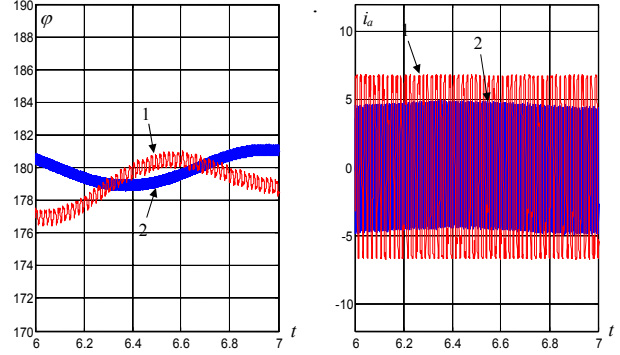


Fig. 3.1: Measured (curve 1) and simulated quantities (curve 2) at the stability boundary for the pole placement controller

The design parameters are now r and q_e . For a large parameter r , the closed-loop poles are the stable poles of the plant and the mirrored unstable poles of the plant. Thus, the closed-loop poles with the LQ controller are essentially the same as with the pole placement controller and the robustness and performance properties are also very similar.

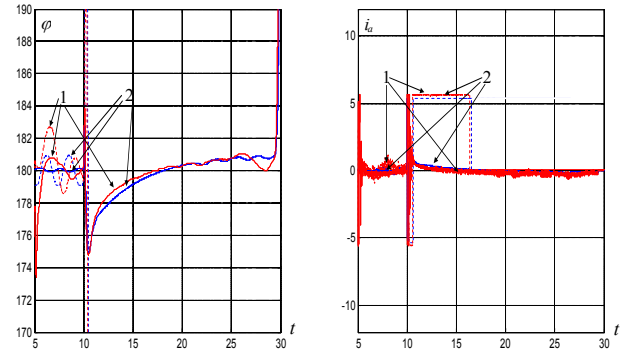


Fig. 3.2: Disturbance rejection with the pole placement and the \mathcal{H}_2 controller (dashed curves: pole placement controller, solid curves: \mathcal{H}_2 controller, curve 1: measured, curve 2: simulated)

Design of a \mathcal{H}_2 controller. The design of a \mathcal{H}_2 controller consists of two parts, namely the design of a LQ controller and a Kalman filter. The poles of the closed-loop system with the LQ controller are not affected by the Kalman filter which is in contrast to the observer described by the differentiators. We use for the LQ cost criterion a large parameter r as above. For the design of the Kalman filter we have to specify sensor noise and plant noise. For the sensor noise, we take exactly the sensor noise which is physically given for the encoders. There is no physically existing source for plant noise. So, for designing the Kalman filter, we introduce artificially noise into the plant which is only used for design purposes. We suppose that there exist for both revolution points stochastic moments which are distributed as white noise. For design purposes, it suffices to use equal spectral densities σ_w . Then σ_w is the only design parameter for the Kalman filter. If σ_w is large, the

\mathcal{H}_2 controller behaves very similar to the LQ controller and has its nice Nyquist curve but is sensitive to the IdHFDyn. If σ_w is small, the controller is insensitive to the IdHFDyn but the Nyquist curve degrades and the controller gets other undesirable properties. A reasonable compromise has to be found by trial and error.

Figure 3.2 shows the result for a disturbance at the plant input, more precisely, a constant additive voltage of 6V. The LQ controller stabilizes the inverted pendulum but is not able to reject this large disturbance, the pendulum falls down. The \mathcal{H}_2 controller is capable to defeat this disturbance but needs a rather long time to bring back the pendulum in the upward position.

IV. DESIGN OF A \mathcal{H}_∞ CONTROLLER

Our next goal is to design a \mathcal{H}_∞ controller. To this end, we weight the transfer functions S_o , KS_o and GS_o . The latter transfer function is the transfer function from a disturbance at the plant input to the variable to be controlled. By this way it is possible influence directly the disturbance rejection properties of the closed-loop system. Figure 4.1 shows the corresponding weighting scheme. The dashed uncertainty block has not to be taken into account.

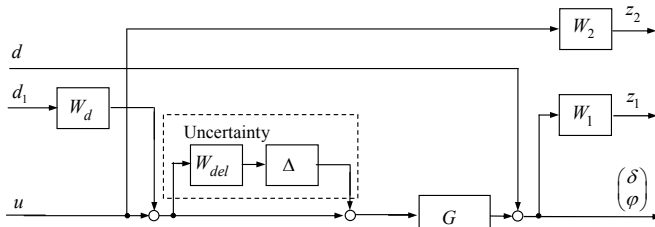


Fig. 4.1: Weighting scheme for the design of the \mathcal{H}_∞ controller and the μ controller

If the extended plant of Fig. 4.1 is controlled by a controller K , then the transfer functions for the closed-loop system are

$$\begin{aligned}\hat{z}_1 &= W_1 S_o \hat{d} + W_1 S_o G W_d \hat{d}_1 \\ \hat{z}_2 &= -W_2 K S_o \hat{d} - W_2 T_i G W_d \hat{d}_1.\end{aligned}$$

Here, S_o is the output sensitivity function and T_i is the input complementary sensitivity function. The choice of the weights is not quite obvious. One possible way to define them is to look at the Bode plots of S_o and KS_o for the \mathcal{H}_2 controller. This gives a reason to choose the weights in the following form: Let $W_1(s) = \text{diag}(w_1(s), w_1(s))$ and

$$w_1^{-1}(s) = k_1 \frac{(s + \omega_{Z1})(s + \omega_{Z2})}{(s + \omega_{N1})(s + \omega_{N2})} \text{ where } \omega_{Z2} = \frac{\omega_{N1}\omega_{N2}}{\omega_{Z1}},$$

$$W_2^{-1}(s) = k_2 \frac{\omega_N}{\omega_{Z\infty}} \frac{s + \omega_{Z\infty}}{s + \omega_N} \text{ with } \omega_{Z\infty} = 100\omega_N.$$

By this way, S_o and KS_o can be formed. Moreover, a nice property of the \mathcal{H}_∞ design is that we now have the chance to form GS_o directly. This will be done by an additional weight W_d which is chosen as a constant (cf. Fig. 4.1). Figure 4.2 depicts the Bode plots of GS_o and T_i for various controllers. The plot shows that the disturbance rejection properties with the \mathcal{H}_∞ controller are considerably better than that of the other controllers. Another important difference is the behavior of T_i for large frequencies. The Bode plot for T_i with the \mathcal{H}_∞ controller rolls off with 80 dB per decade. For the \mathcal{H}_2 controller, this amount reduces 60 dB per decade and for the pole placement controller this amount reduces further to 40 dB per decade. This is why the pole placement controller is so sensitive against the IdHFDyn.

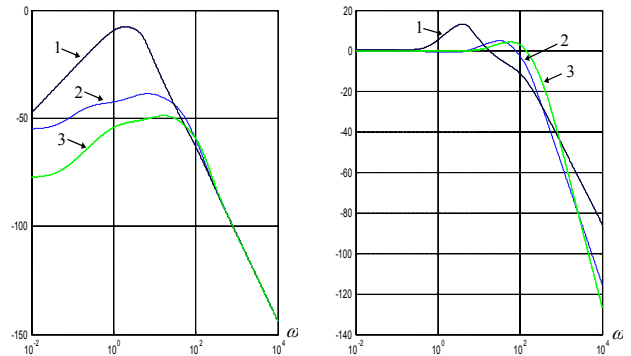


Fig. 4.2: Singular value plot of GS_o (left-hand figure) and T_i (right-hand figure) for the pole placement controller (1), the \mathcal{H}_2 controller (2) and the \mathcal{H}_∞ controller (3)

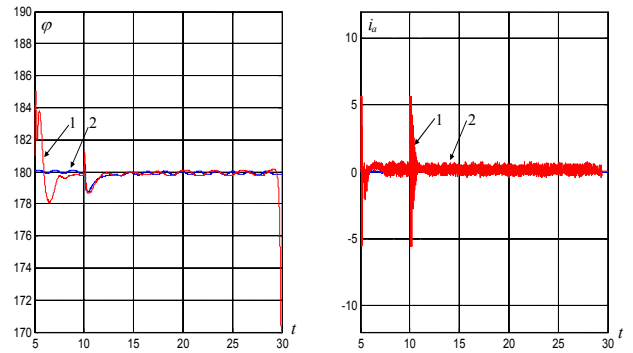


Fig. 4.3: Disturbance rejection with the \mathcal{H}_∞ controller (curve 1: measured, curve 2: simulated)

Figure 4.3 shows the response to a disturbance of the closed-loop system with the \mathcal{H}_∞ controller. From this figure it can be seen that the disturbance rejection properties for the \mathcal{H}_∞ controller are in fact considerably better than for the \mathcal{H}_2 controller (cf. Fig. 3.2).

We now strengthen our requirements for the controller in the sense that we add a further uncertainty to the plant. Beside to the IdHFDyn we introduce artificially uncertainty by adding at the input of the pwm amplifier an electronic circuit like an all-pass. Denote its transfer function by G_{el} .

Then the transfer function of the plant can be written in the form $G_p = (1 + W_\Delta \Delta)G$ with an arbitrary stable transfer function Δ such that $\|\Delta\|_\infty \leq 1$. The weight W_Δ has to be chosen such that G_{cl} takes the form $1 + W_\Delta \Delta$. We define (with $k_1 = 0.001$, $\omega^* = 300$, $W_\infty = 1$)

$$W_\Delta(s) = W_\infty \frac{s + \omega^* k}{s + \omega^* W_\infty}.$$

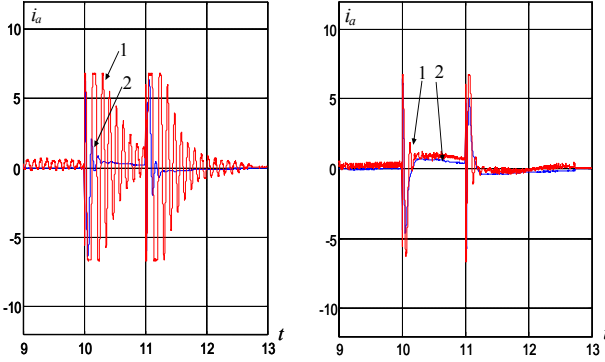


Fig. 4.4: Disturbance rejection under model uncertainty, \mathcal{H}_∞ controller (left-hand figure) and μ controller (right-hand figure), (1: measured, 2: simulated)

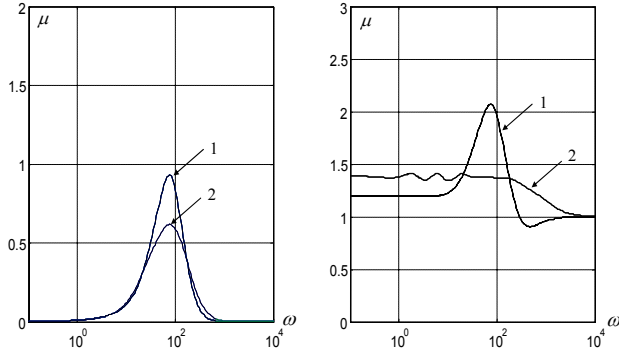


Fig. 4.5: Robust stability (left-hand figure) and robust performance (right-hand figure) for the \mathcal{H}_∞ controller (1) and the μ controller (2)

By using the D-K iteration it is possible to synthesize a controller which has robust performance for all plants belonging to this set. The weighting scheme of Fig. 4.1 has then to be considered with the robustness weight W_Δ . Figure 4.4 shows the responses of the current for the resulting μ controller and the \mathcal{H}_∞ controller for an additional all-pass with a time constant of $T_A = 0.004s$. The improvement can clearly be seen. Using μ tools, the robust stability and robust performance properties of the \mathcal{H}_∞ controller and the μ controller can be compared (cf. Fig 4.5).

V. REJECTION OF AN OSCILLATORY DISTURBANCE

Finally, assume that the horizontal bar with the additional pendulum with a spring is attached to the pendulum, as described in Sect. 2. By this way, the plant dynamics changes considerably. First, suppose that the two additional

masses are fixed at the horizontal rod. Then the moment of inertia of the upper pendulum and its length l_1 are changed. By this way, we get the nominal plant for which the controllers are designed. The additional dynamics due to the spring is only taken into account for simulation purposes but not for controller design. The linearized differential equation for the rotation about D_1 is

$$m_2 l_2 L \ddot{\psi} + J_1 \ddot{\phi} - (m_1 l_1 + m_2 L) g \phi = m_0 L_0 \ddot{z} + M_a.$$

Here, the term $m_0 L_0 \ddot{z}$ can be viewed as an oscillatory disturbance moment. The linearized differential equation for the spring is

$$m_0 L_0 \ddot{\phi} + m_0 \ddot{z} + cz = 0.$$

The point is that ϕ enters also into the differential equation for z . By this way, the spring dynamics and the double pendulum dynamics are coupled and if a controller has been designed only for the double pendulum, the closed-loop system with the spring may become unstable. The closed-loop poles corresponding to the double pendulum are only moderately shifted but the poles of the spring which lie on the imaginary axis may move either in the negative or the positive half-plane. In the latter case, the amplitude of the spring oscillation increases until it reaches

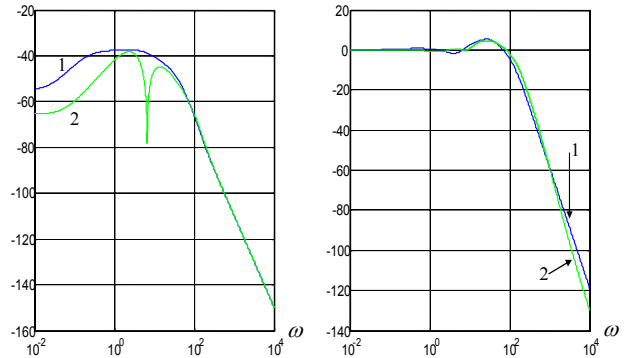


Fig. 5.1: Singular value plot of GS_o (left-hand figure) and T_l (right-hand figure) for the \mathcal{H}_2 controller (1) and the \mathcal{H}_∞ controller with the dynamic weight W_d (2)

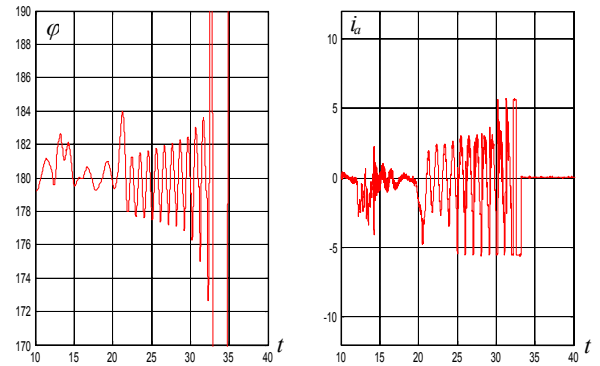


Fig. 5.2: Disturbance rejection with the spring: unstable case, \mathcal{H}_2 controller

the physical limits (or the pendulum falls down).

Our design goal is now to synthesize a controller which has the following properties:

1. The closed-loop poles corresponding to the double pendulum are only moderately shifted by the spring dynamics.
2. The closed-loop poles corresponding to the spring get a small positive damping.
3. The controller is capable to reject almost completely an oscillatory disturbance of maximum amplitude caused by the spring.

These criteria can be checked for the various controllers. The pole placement controller fulfils the criteria 1 and 2 but not 3, and the \mathcal{H}_2 controller fails since he doesn't fulfill criterion 2: The closed-loop poles corresponding to the spring get a negative damping. This can also be seen from the measured angle φ and the current, cf. Fig. 5.2: The spring is deflected manually after approximately 22s. Then the amplitude of the spring oscillation increases and the same does the oscillation of φ until the pendulum falls down after approximately 33s. The \mathcal{H}_∞ controller fulfils 1 and 2 if the weights are properly chosen but criterion 3 only to some extend.

To get a really convincing result, the choice of W_d has to be refined. One possibility is to use a weight which works like a notch filter. Let

$$W_d = w_d \frac{s^2 + 2\omega_s s + \omega_s^2}{s^2 + 2d_N \omega_s s + \omega_s^2}$$

where ω_s is close to the eigenfrequency of the spring-mass system and where the damping d_N is relatively small ($d_N = 0.3$, e.g.). The problem with this weight is that it has a certain tendency to make the closed-loop system unstable. The instability can be avoided by choosing the weight W_2 such that $|T_i|$ is not too large in a vicinity of the eigenfrequency of the spring. The corresponding magnitude plots of transfer function for the disturbance and T_i are shown in Fig. 5.1. The \mathcal{H}_∞ controller has now very

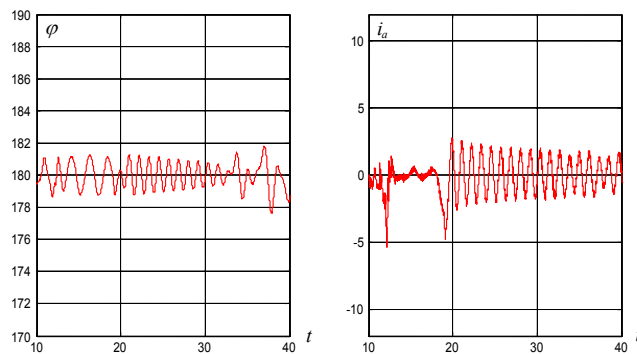


Fig. 5.3: Disturbance rejection with the spring: stable case, \mathcal{H}_∞ controller and dynamic weight W_d .

good disturbance rejection properties and the system remains stable in the presence of the spring. The experiment convincingly shows the benefits of this refined \mathcal{H}_∞ design, cf. Fig. 5.3: The spring is taken manually to its maximum deflection after approximately 20s and the oscillations are almost completely suppressed. What is visible is a superposition of the permanent oscillations due to Coulomb friction and the small contribution of the spring oscillations. The amplitude of the sum of both is not larger than the contribution coming only from the Coulomb friction. It can also clearly be seen that the closed-loop system is stable.

The PendCon Family. We would like to mention that this experiment belongs to a family of experiments which we have designed for education and research purposes at the Laboratory for Control Systems in the Department of Mechanical Engineering of the Fachhochschule Lübeck (University of Applied Sciences). There are experiments of an elementary character which suit very well to an introductory course on control system design as well experiments of an advanced level. The interested reader may visit the homepage www.pendcon.de, where also additional information about the experimental set-up can be found. There are also many instructive short films presented. Four of them belong to the experiment described in this paper:

- Inverted pendulum where the linear closed-loop system is unstable but where the pendulum doesn't fall down (cf. Fig. 3.1).
- Disturbance rejection for the uncertain pendulum with the \mathcal{H}_∞ controller and the μ controller (cf. Fig. 4.4).
- Rejection of an oscillatory disturbance with the \mathcal{H}_2 controller (cf. Fig. 5.2).
- Rejection of an oscillatory disturbance with the \mathcal{H}_∞ controller (cf. Fig. 5.3).

VI. REFERENCES

- [1] Balas, G., Chiang, R., Packard, A., Safanov, M.: *Robust Control Toolbox*, The MathWorks, Naticks, 2005.
- [2] Delibasi, A., Kucukdemiral, I., Cansever, G.: A robust PID like state-feedback control via LMI approach: An application on a double inverted pendulum system, Proceedings of the International Symposium on Computational Intelligence in Robotics and Automation, pp. 374-379, 2007.
- [3] Kawaji, S., Kanazawa, K.: Control of double inverted pendulum with elastic joint, Proceedings of the Intelligence for Mechanical Systems Workshop, pp. 946-951, 1991.
- [4] Niemann, H., Poulsen, J.: Design and analysis of controllers for a double inverted pendulum, Proceedings of the American Control Conference, pp. 2803-2808, 2003.
- [5] Mackenroth, U.: Robust control of a laboratory pendulum with uncertain high frequency dynamics, Proceedings of the European Control Conference, pp. 2694 - 2700, Kos (Greece), 2007.
- [6] Wie, B., Liu, Q. and Bauer, F.: Classical and robust \mathcal{H}_∞ control design for the Hubble space telescope, J. Guid. Control Dyn., **16**, 1069-1077, 1993.
- [7] Zhou, K., Doyle, J. and Glover, K.: *Robust and Optimal Control*, Prentice Hall, Englewood Cliffs, New Jersey, 1995.